Available online at www.sciencedirect.com
ScienceDirect
Trans. Nonferrous Met. Soc. China 31(2021) 3691−3702
Transactions of Nonferrous Metals Society of China
www.tnmsc.cn

# Effect of Y on microstructure evolution and mechanical properties of Mg−4Li−3Al alloys

Li-li CHANG, Jing GUO, Xiao-jing SU

School of Materials Science and Engineering, Shandong University, Ji'nan 250061, China

Received 13 November 2020; accepted 30 July 2021

**Abstract:** To obtain magnesium alloys with a low density and improved mechanical properties, Y element was added into Mg−4Li−3Al (wt.%) alloys, and the effect of Y content on microstructure evolution and mechanical properties was investigated by using optical microscopy, scanning electron microscopy and tensile tests. The results show that mechanical properties of as-cast Mg−4Li−3Al alloys with Y addition are significantly improved as a result of hot extrusion. The best comprehensive mechanical properties are obtained in hot-extruded Mg−4Li−3Al−1.5Y alloy, which possesses high ultimate tensile strength (UTS=248 MPa) and elongation ($\delta$=27%). The improvement of mechanical properties of hot-extruded Mg−4Li−3Al−1.5Y alloy was mainly attributed to combined effects of grain refinement, solid solution strengthening and precipitation strengthening.

**Key words:** Mg−Li−Al alloy; Y element; microstructure; ultimate tensile strength; elongation

## 1 Introduction

Mg−Li alloys are the lightest engineering metals, and they were widely used in military, aerospace, automobile and 3C industries due to their low density, high specific strength and stiffness, good electromagnetic shielding performance and excellent damping. However, the poor strength impeded the potential and wide applications of Mg−Li alloys [1−6]. Alloying is a convenient but effective approach of improving the strength of metals through solid solution hardening, precipitation hardening and refinement strengthening mechanisms. A variety of elements, such as Al, Zn, Sn, Ca and rare earth (RE) elements have been added into Mg−Li alloys to improve mechanical properties in Mg−Li alloys [1−12]. Al addition has been proven to lead to remarkable age hardening, caused by hardening of the $\alpha$-phase with AlLi and $Mg_{17}Al_{12}$ precipitates in Mg−Li alloys [1,13−15]. In order to further improve the strength and ductility of Mg−Li−Al alloys, additional alloying is needed. Rare earth (RE) elements have been reported to improve the strength, formability and corrosion resistance of Mg−Li alloys effectively by solid solution hardening, grain refinement strengthening and second phase hardening due to the formation of Al−RE compounds [8,16−19]. Among RE elements, yttrium (Y) has been reported to be an effective and excellent strengthening modifier for Mg−Li alloys [3]. Adding only a small amount of Y can significantly improve the mechanical properties of magnesium alloys [2,7]. CUI et al [3] stated that adding Y to Mg−5Li−3Al−2Zn results in the formation of $Al_2Y$ compound and facilitates grain refinement. According to their results of tensile test, the additions of Y can improve the mechanical properties of the alloy. DONG et al [2] investigated the effect of Y on microstructure and mechanical properties of duplex Mg−7Li alloys and found that

**Corresponding author:** Li-li CHANG, Tel: +86-531-88392315, E-mail: lilichang@sdu.edu.cn
DOI: 10.1016/S1003-6326(21)65757-6

the strength of the alloy was enhanced by adding Y element, and the elongation was improved with the Y content of no more than 3 wt.% [2]. HANTZSCHE et al [20] confirmed that magnesium sheets with weak textures were achievable by using alloying elements such as Nd, Ce and Y. Due to the reasons mentioned above, Al and Y were selected to be alloying elements for Mg−Li alloys. In the present study, Mg−4Li−3Al alloys with different Y contents were prepared by vacuum melting and hot extrusion, and the effect of Y on microstructure evolution and mechanical properties of Mg−Li−Al alloys was investigated and discussed.

## 2 Experimental

Pure Mg (99.99 wt.%) and Mg−25wt.%Y master alloy were put into graphite crucible and melted in a vacuum mid-frequency induction furnace (ZG−10). The molten alloy was cast into a steel mold (*d*55 mm × 180 mm). In order to separate the ingot and mold easily and improve the surface quality of the ingot, a layer of boron nitride release agent was sprayed on the inner surface of the steel mold. Argon gas was used to avoid the oxidation of Mg−Li alloy melt during melting and casting processes. The casting temperature was kept in the range of 650−750 °C during casting. The chemical compositions of Mg−4Li−3Al alloys were determined by inductively coupled plasma atomic emission spectroscopy (ICP-AES), and the results are summarized in Table 1.

**Table 1** Chemical compositions of Mg−Li−Al alloys (wt.%)

| Alloy | Al | Li | Y | Mg |
|---|---|---|---|---|
| Mg−4Li−3Al | 2.98 | 3.72 | − | Bal. |
| Mg−4Li−3Al−0.5Y | 3.23 | 4.12 | 0.46 | Bal. |
| Mg−4Li−3Al−1Y | 3.04 | 4.24 | 0.88 | Bal. |
| Mg−4Li−3Al−1.5Y | 3.10 | 4.18 | 1.3 | Bal. |
| Mg−4Li−3Al−2Y | 2.98 | 3.79 | 2.32 | Bal. |

For hot extrusion, billets with a diameter of 40 mm and a height of 60 mm were machined from the central part of Mg−4Li−3Al ingots with different Y contents. The surface of the cylindrical samples for hot-extrusion was ground with sandpaper. The billet was preheated at 300 °C for 5 min, and then extruded to be a *d*10 mm bar in a vertical extruder (YAW−3000). Parameters of extrusion process are given in Table 2.

**Table 2** Parameters of extrusion process

| Extrusion temperature/ °C | extrusion speed/ ($mm \cdot s^{-1}$) | extrusion ratio | Preheating temperature/ °C |
|---|---|---|---|
| 300 | 3 | 16:1 | 300 |

Samples for microstructure observation were cut form ingots and extrudates, ground with sandpapers and mechanically polished with polishing pastes. Optical microstructure was revealed by a picric acid solution (6 g picric acid + 70 mL anhydrous ethanol + 10 mL glacial acetic acid + 10 mL distilled water) and observed under a microscope (Nikon MA−100). Secondary electron images of Mg−4Li−3Al alloys were obtained by using the QUANT200 scanning electron microscope (SEM). Qualitative analysis of the elemental composition and content of the precipitated particles was performed by energy dispersive spectrometer (EDS). X-ray diffraction for phase determination was conducted with Cu $K_\alpha$ radiation source at an accelerating voltage of 36 kV. The step size of diffraction angle is 0.02°, the scanning speed is 4 (°)/min and the scanning range of $2\theta$ is 5°−95°. The equipment (Bruker D8 advance) was used to carry out a macro-texture test on the extruded sample, and the sample surface was perpendicular to the extrusion direction (ED). Four incomplete pole figures $\{0002\}$, $\{10\bar{1}0\}$, $\{10\bar{1}1\}$, and $\{10\bar{1}2\}$ in the $\alpha$-Mg phase were measured, and the series expansion method was used to get the complete pole figures. A field emission scanning electron microscope (JSM-7800F) equipped with an EBSD system was used to characterize the microstructure and micro-texture of the extruded Mg−4Li−3Al alloys. The observation surface for EBSD analysis was the ED−TD plane. The working voltage and current were 20 kV and the 40 mA, respectively. Data processing was conducted by using Channel 5 software. The specimens for tensile tests were flat pieces with the gauge size of 10 mm × 3 mm × 2 mm and tensile tests were conducted on an electronic universal testing machine (WDW−200E) at room temperature with a strain rate of $1\times10^{-3}$ $s^{-1}$.

## 3 Results

Figure 1 shows the optical microstructures of as-cast Mg−4Li−3Al alloys with different Y contents. The as-cast Mg−4Li−3Al alloys are composed of $\alpha$-Mg matrix with equiaxed grains and second phases (black points in images). According to their shapes, these second phases in Mg−4Li−3Al alloys can be divided into two types: second phases with irregular shapes distributing along the network of grain boundaries marked with arrow A in Fig. 1(a) and circular black particles noted as arrow with B in Fig. 1(b) distributing homogeneously at grain boundaries and grain interior. The area fraction of second phases with irregular shapes decreases with increasing Y content in Mg−4Li−3Al alloys, while the amount of circular second phases increases as Y content increases. Meanwhile, it should be noted that with increasing Y content in Mg−4Li−3Al alloys, the homogeneous distribution of circular black particles becomes concentrated as clusters, as seen in Fig. 1(e).

The average grain size of as-cast Mg−4Li−3Al with different Y additions was determined by software Image-Pro-Plus, and the results are listed in Table 3. According to Table 3, the average grain size of Mg−4Li−3Al alloy with 0.5 wt.% Y addition is almost the same as that of Mg−4Li−3Al alloy without Y addition. When the Y content is increased to 1 wt.%, grains of Mg−4Li−3Al ingot are refined from ~127 to ~110 μm. However, when the Y content is greater than 1 wt.%, the average grain size does not decrease as the Y content increases.

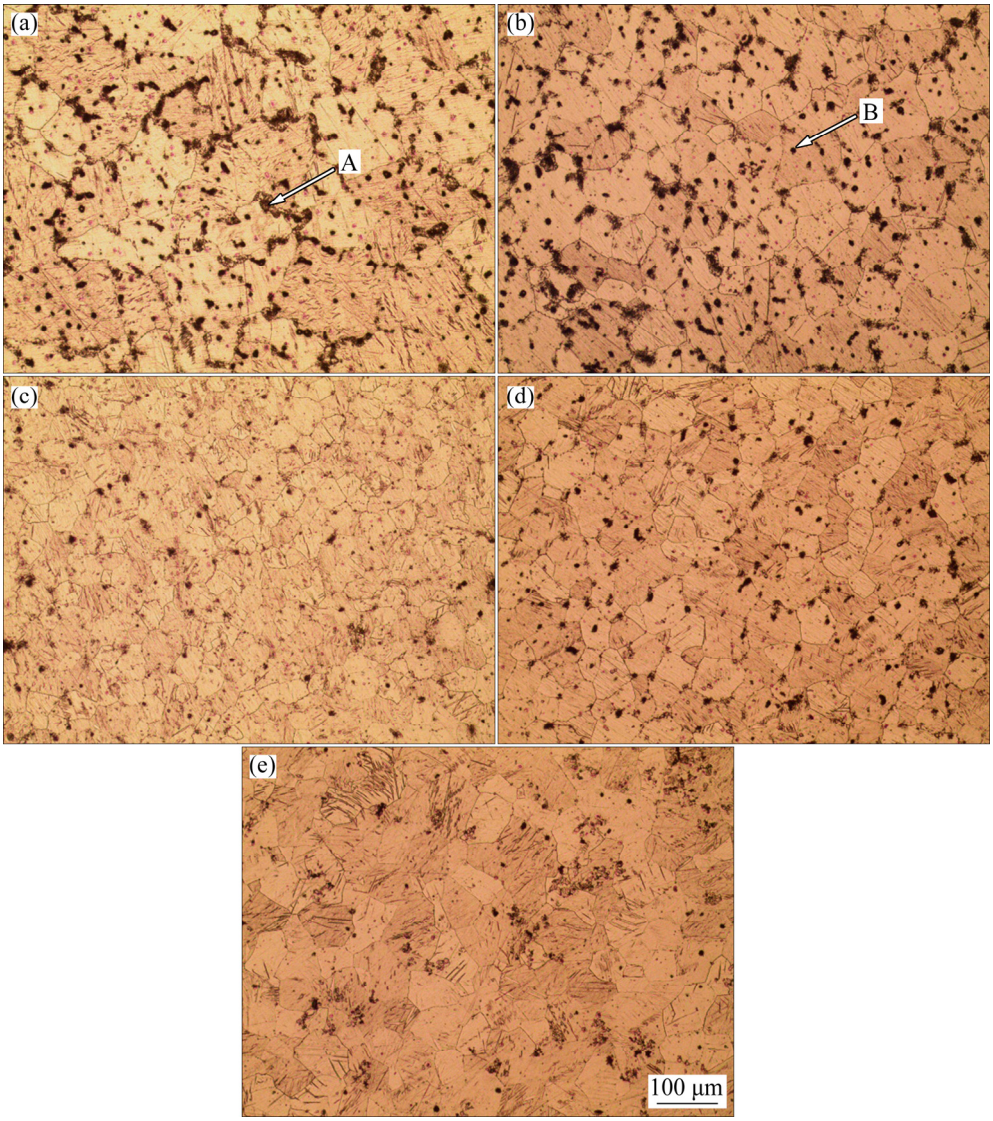


**Fig. 1** Optical microstructures of as-cast Mg−4Li−3Al alloys with different Y additions: (a) 0Y; (b) 0.5Y; (c) 1Y; (d) 1.5Y; (e) 2Y

**Table 3** Average grain size of as-cast and hot-extruded Mg−4Li−3Al alloys

| Alloy | Average grain size/μm | |
|---|---|---|
| | As-cast | Extruded |
| Mg−4Li−3Al | 126.7±3 | 11.5±0.5 |
| Mg−4Li−3Al−0.5Y | 127.4±3 | 10.7±0.5 |
| Mg−4Li−3Al−1Y | 110.5±5 | 11.3±0.5 |
| Mg−4Li−3Al−1.5Y | 110.5±4 | 8.5±1 |
| Mg−4Li−3Al−2Y | 111.2±2 | 14.0±1 |

Hence, the average grain size results in Table 3 indicate that there is a critical value of Y addition to produce grain refinement effect in Mg−4Li−3Al alloys (1 wt.% in the present study), and the average grain size cannot decrease further when the Y addition is more than 1 wt.%.

In order to distinguish second particles in Mg−4Li−3Al alloys, microstructures were observed by SEM under higher magnification and second phases were confirmed by point and map scanning using EDS. SEM images and EDS results of as-cast Mg−4Li−3Al alloys with 0.5 wt.% Y addition are shown in Fig. 2. The compositions of Points A, B and C in Fig. 2(a) are summarized in Table 4. Combination of Fig. 2 and Table 4 indicates that $Al_2Y$, $MgLi_2Al$ and $Mg_{17}Al_{12}$ exist in as-cast Mg−4Li−3Al−0.5Y alloy. Due to the limitation of SEM technique, AlLi particles are not distinguished by EDS. However, AlLi phase is recognized by XRD in Fig. 3.

Microstructures of as-cast Mg−4Li−3Al alloys were observed by SEM under higher magnification and SEM images of as-cast Mg−4Li−3Al alloys with different Y additions are shown in Fig. 4. As seen in Fig. 4, $Mg_{17}Al_{12}$, $MgLi_2Al$ and AlLi phases are observed in Mg−4Li−3Al alloys. After Y addition, $Al_2Y$ particles are characterized, as seen in Fig. 4(d). According to SEM images, rod-like $MgLi_2Al$ phase distributes along grain boundaries; filamentous $Mg_{17}Al_{12}$ phase is mostly formed along grain boundaries and rarely locates inside grains; white particles along grain boundaries are confirmed to be AlLi phase while intragranular white particles are characterized to be $Al_2Y$. Figure 4 shows that the amount of $Mg_{17}Al_{12}$ and $MgLi_2Al$ phases decreases with increasing Y content in Mg−4Li−3Al alloys, while the particle size and amount of $Al_2Y$ increase with increasing Y content. Therefore, it can be induced that most Al element is consumed to form $Al_2Y$ particles when Y is added, thus reducing the number of other phases containing Al, such as $Mg_{17}Al_{12}$ and $MgLi_2Al$.

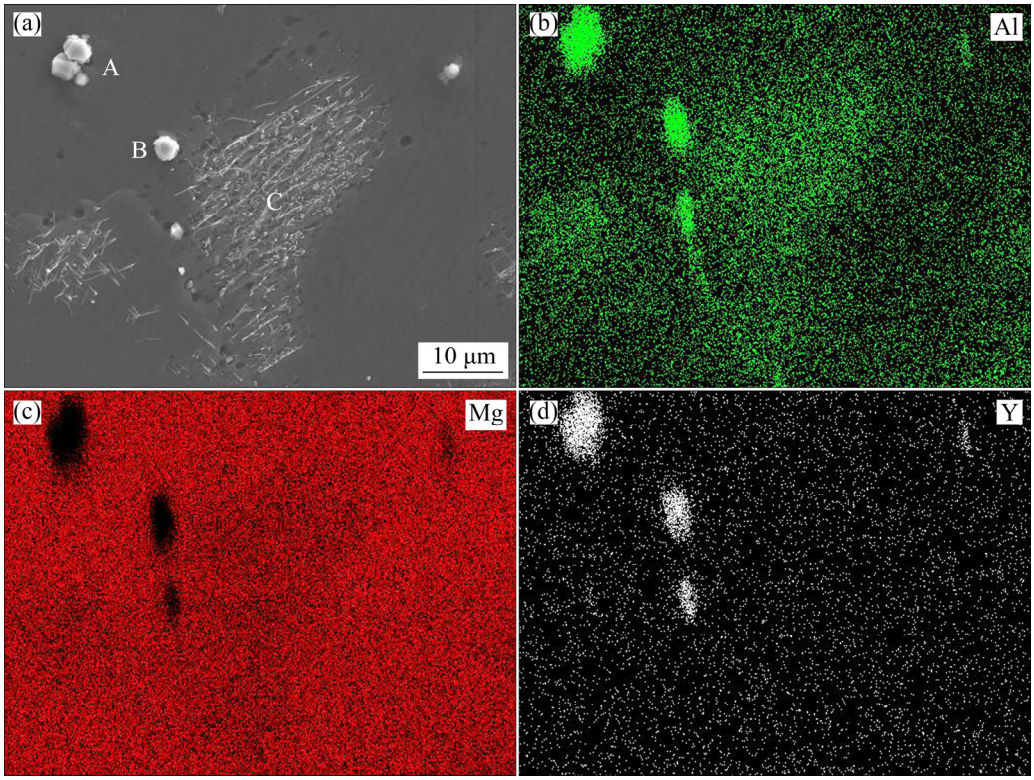


**Fig. 2** SEM image and EDS element maps of as-cast Mg−4Li−3Al−0.5Y alloy: (a) SEM image; (b) Al; (c) Mg; (d) Y

**Table 4** Chemical compositions of different particles in as-cast Mg−4Li−3Al−0.5Y alloys (at.%)

| Phase | Mg | Al | Y |
|---|---|---|---|
| A ($Al_2Y$) | 34.34 | 33.28 | 15.45 |
| B ($MgLi_2Al$) | 76.76 | 7.37 | – |
| C ($Mg_{17}Al_{12}$) | 92.08 | 7.92 | – |

Figure 3 presents XRD patterns of as-cast and extruded Mg−4Li−3Al alloys with different Y additions. According to Fig. 3(a), the as-cast Mg−4Li−3Al alloy without Y addition is composed of $\alpha$-Mg, $Mg_{17}Al_{12}$, $MgLi_2Al$ and AlLi phases. When Y is added into Mg−4Li−3Al alloy, peaks of $Al_2Y$ are detected and the intensities of $Al_2Y$ peaks

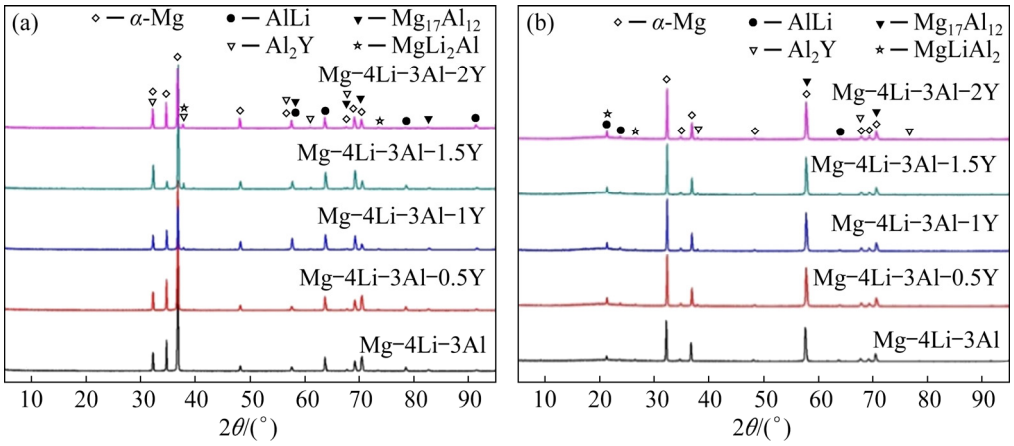


**Fig. 3** XRD patterns of Mg−4Li−3Al alloys: (a) As-cast; (b) Hot-extruded

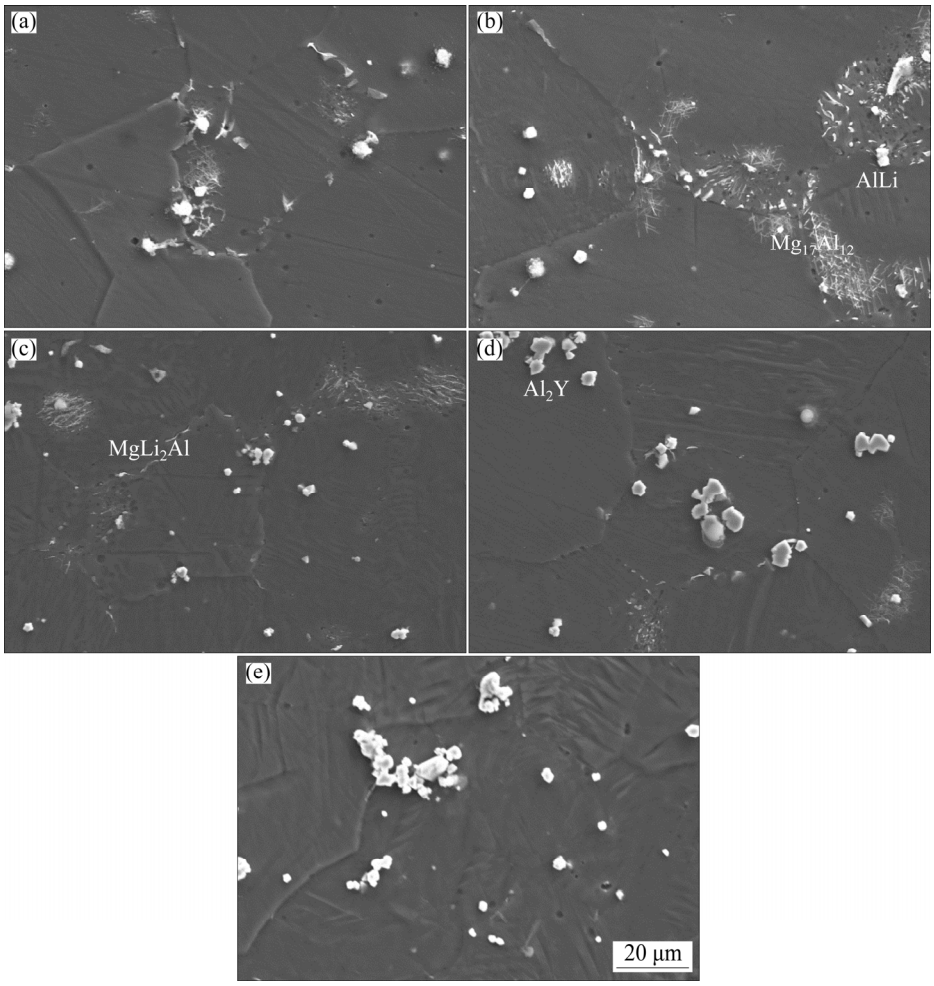


**Fig. 4** SEM images of as-cast Mg−4Li−3Al alloys with different Y additions: (a) 0Y; (b) 0.5Y; (c) 1Y; (d) 1.5Y; (e) 2Y

become higher with increasing Y addition. After hot extrusion, XRD peaks of $MgLi_2Al$ fail to appear while $MgLiAl_2$ phase is detected, revealing that the metastable $MgLi_2Al$ phase is changed to be a stable $MgLiAl_2$. Although previous report indicated that the metastable $MgLi_2Al$ phase transformed to a stable $MgLiAl_2$ phase during aging at higher temperatures or for longer durations [21], $MgLi_2Al$ phase was found in the studied Mg−4Li−3Al alloys. Instead of the $MgLi_2Al$ phase, the precipitation of $MgLiAl_2$ phase has also been detected in Mg−14Li−1Al alloy during the process of equal channel angular extrusion at room temperature [22]. $Al_2Y$ is a hard compound with a high melting point of 1758 K, $MgLi_2Al$ is a metastable strengthening phase which can transform to a stable $MgLiAl_2$ phase during hot extrusion, and $Mg_{17}Al_{12}$ phase is also a strengthening phase in magnesium alloys containing Al element. Therefore, the enhancement of strength of Mg−4Li−3Al alloys with Y addition can be achieved by second phase strengthening due to the existence of $Al_2Y$, $MgLi_2Al$ ($MgLiAl_2$), and $Mg_{17}Al_{12}$ intermetallic compounds.

Optical microstructures of hot-extruded Mg−4Li−3Al alloys with different Y additions are shown in Fig. 5 and the average grain sizes determined by Image-Pro-Plus are illustrated in Table 3. As seen in Fig. 5, typical recrystallized microstructures with equiaxed grains are observed in hot-extruded Mg−4Li−3Al alloys, indicating dynamic recrystallization occurs during hot extrusion. By comparing Fig. 1 and Fig. 5, it is found that grains of Mg−4Li−3Al ingots are refined significantly due to the dynamic recrystallization

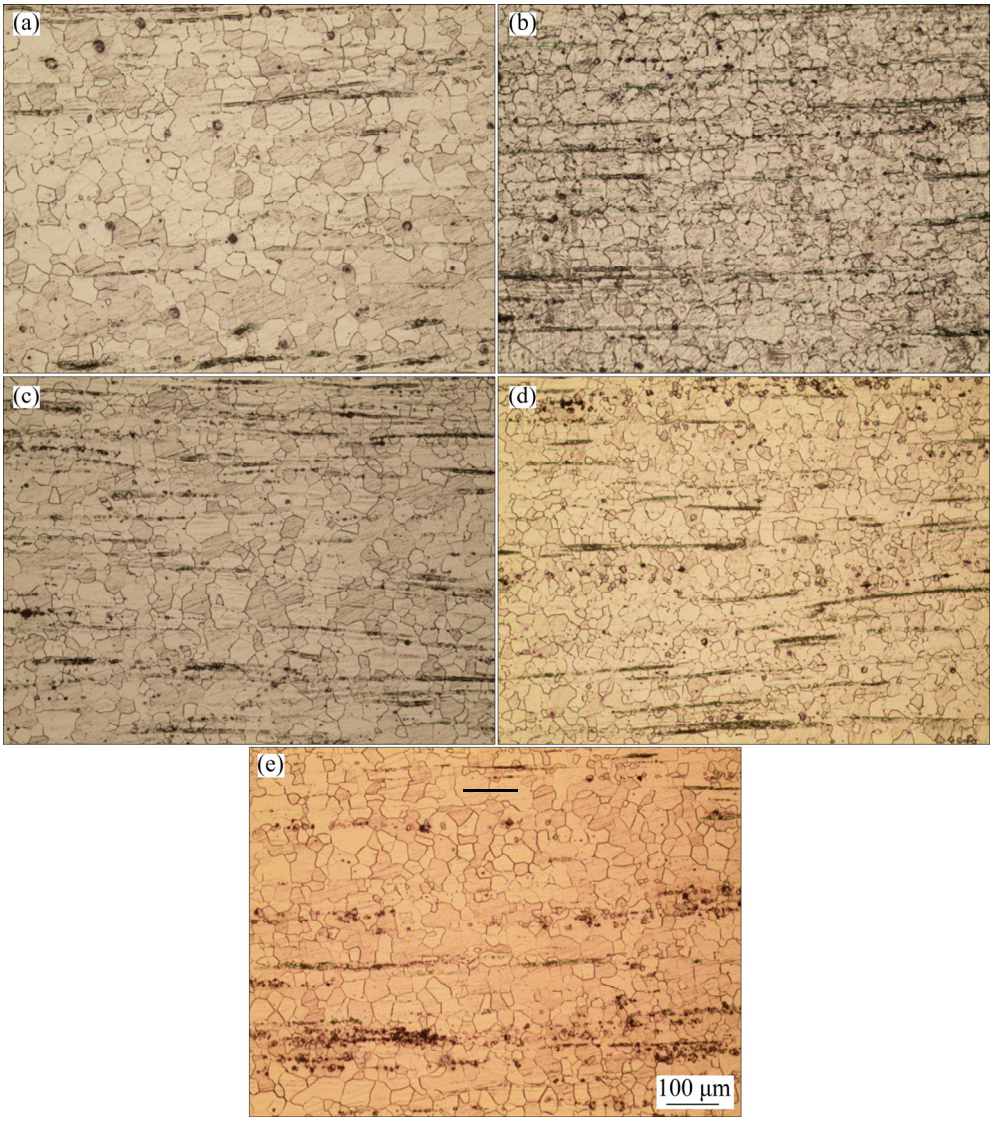


**Fig. 5** Optical microstructures of hot-extruded Mg−4Li−3Al alloys: (a) Mg−4Li−3Al; (b) Mg−4Li−3Al−0.5Y; (c) Mg−4Li−3Al−1Y; (d) Mg−4Li−3Al−1.5Y; (e) Mg−4Li−3Al−2Y

(DRX) during hot extrusion process and the average grain size of hot extruded Mg−4Li−3Al−1.5Y alloy is the smallest. It should be noted that although the average grain size of Mg−4Li−3Al−0.5Y and Mg−4Li−3Al ingots is almost the same (~127 μm), the average grain size of hot-extruded Mg−4Li−3Al−0.5Y is surprisingly finer. Besides grain refinement, the redistribution of second phases is observed. As shown in Fig. 5, second phases presenting as black stripes align along ED. Further investigation of second phase distribution according to Fig. 5 indicates that the particle size of Mg−4Li−3Al is much larger than that of other alloys, while the amount of second phases in Mg−4Li−3Al−1Y is the highest. Moreover, large particles with a higher volume fraction are observed in Mg−4Li−3Al with 2 wt.% Y addition, while fine particles with a lower volume fraction are found in Mg−4Li−3Al alloys with 0.5 and 1.5 wt.% Y addition.

Figure 6 displays EBSD maps of hot-extruded Mg−4Li−3Al alloys with different Y contents. As seen in EBSD maps, equiaxed grains are observed in hot-extruded Mg−4Li−3Al alloys as a result of DRX during hot extrusion. According to Fig. 6, the average grain size of Mg−4Li−3Al alloys decreases slightly with increasing Y content and reaches a minimum of 8.5 μm with 1.5 wt.% Y addition. When the Y content increases to 2.0 wt.%, the average grain size gets a maximum of ~14 μm. Therefore, the average grain size of hot-extruded Mg−4Li−3Al alloys decreases firstly with increasing Y content, gets a minimum of 8.5 μm in Mg−4Li−3Al alloy with 1.5 wt.% Y and then increases as the Y content increases.

IPFs of hot-extruded Mg−4Li−3Al alloys with different Y additions are shown in Fig. 7. As seen in Fig. 7, $\langle 10\bar{1}0\rangle$−$\langle 2\bar{1}\bar{1}0\rangle$ fiber texture is observed in hot-extruded Mg−4Li−3Al alloys with and

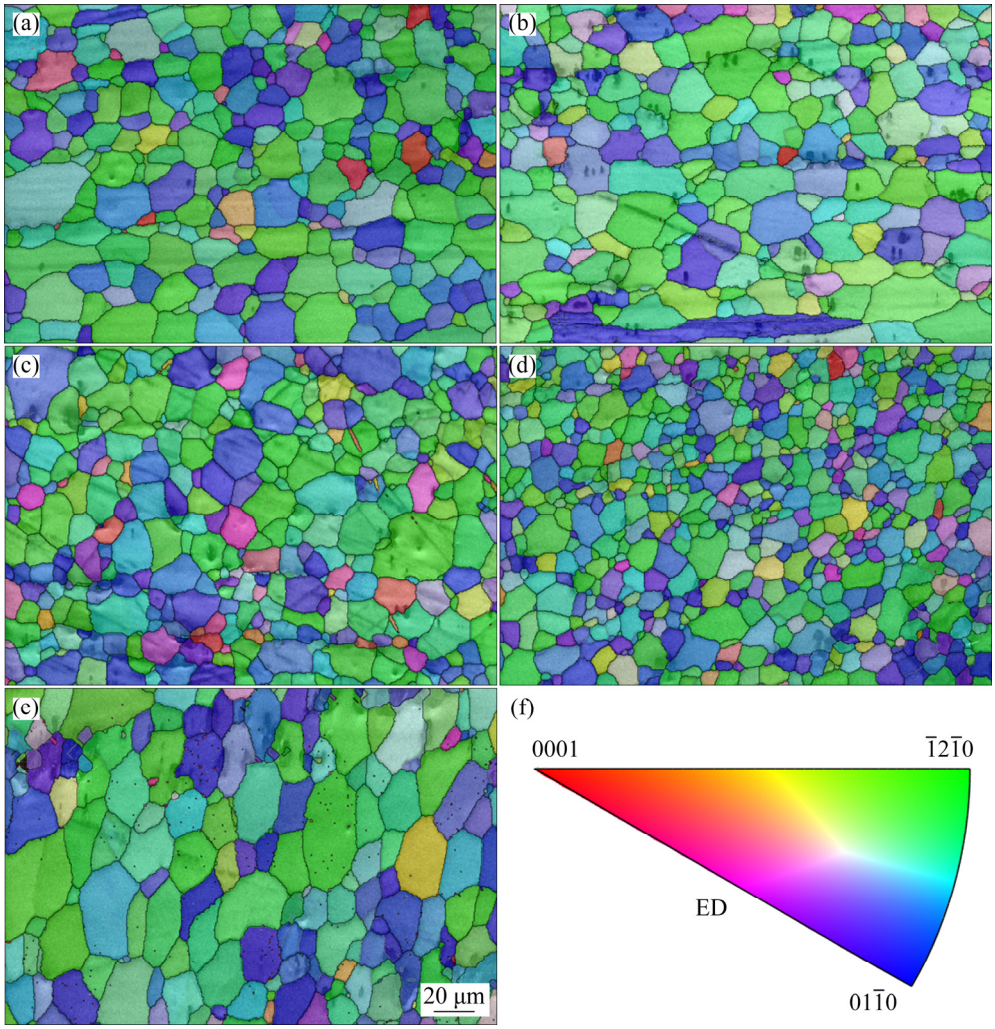


**Fig. 6** EBSD maps of hot-extruded Mg−4Li−3Al alloys with different Y additions: (a) 0Y; (b) 0.5Y; (c) 1Y; (d) 1.5Y; (e) 2Y; (f) IPF color code

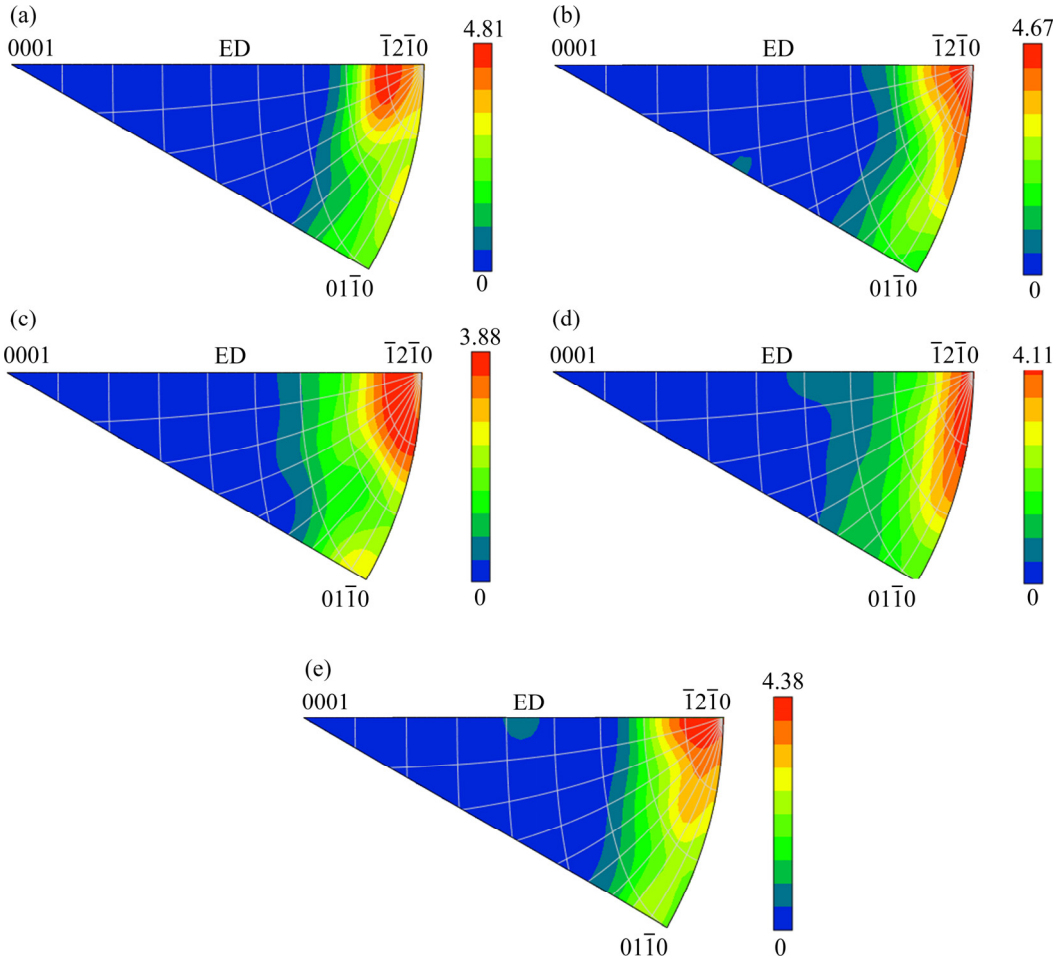


**Fig. 7** IPFs of hot-extruded Mg−4Li−3Al alloys with different Y additions: (a) 0Y; (b) 0.5Y; (c) 1Y; (d) 1.5Y; (e) 2Y

without Y addition and the pole intensity is on the similar level. According to the intensity level in Fig. 7, the maximum intensity of $\langle 2\bar{1}\bar{1}0\rangle$ fiber texture (4.81) is obtained in Mg−4Li−3Al with 0.5 wt.% Y addition, while the smallest intensity (3.88) of fiber texture is found in Mg−4Li−3Al alloy with 1.0 wt.% Y. Further investigation of Fig. 7 indicates ED spreads from $\langle 2\bar{1}\bar{1}0\rangle$ towards $\langle 0001\rangle$ and/or $\langle 10\bar{1}0\rangle$ directions depending on varying Y contents in Mg−4Li−3Al alloys.

Figure 8 presents tensile engineering strain−stress curves of as-cast and hot-extruded Mg−4Li−3Al alloys with Y additions and tensile mechanical properties are summarized in Table 5. As seen in Fig. 8, after hot extrusion, both strength and elongation of Mg−4Li−3Al alloys are significantly increased. For as-cast samples, the largest UTS and elongation at failure are 211 MPa and 17.8%, respectively, which are both obtained in Mg−4Li−3Al alloy with 0.5 wt.% Y addition. Tensile engineering strain−stress curves of as-cast Mg−4Li−3Al−1.5Y show almost exactly the same

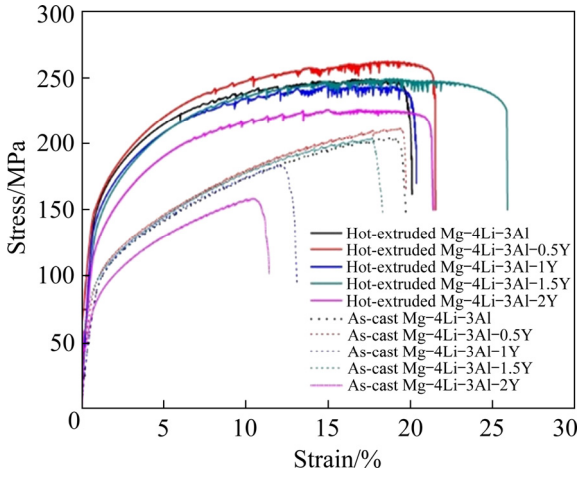


**Fig. 8** Tensile strain−stress curves of Mg−4Li−3Al alloys with different Y additions

shape with Mg−4Li−3Al alloy, and their UTS and elongation are on the same level. However, when the Y content is 2 wt.% Y, both UTS and elongation at room temperature decrease obviously. After hot extrusion, the UTS and elongation are improved

**Table 5** Tensile properties of Mg−4Li−3Al alloys with different Y additions

| Alloy | As-cast | | Hot-extruded | |
|---|---|---|---|---|
| | UTS/MPa | Elongation/% | UTS/MPa | Elongation /% |
| Mg−4Li−3Al | 205±0.7 | 17.5±2.1 | 246±6.5 | 20.0±4.0 |
| Mg−4Li−3Al−0.5Y | 211±9.1 | 17.8±0.2 | 259±2.0 | 22.8±1.8 |
| Mg−4Li−3Al−1Y | 183±10.2 | 11.8±1.1 | 244±10.8 | 20.5±5.0 |
| Mg−4Li−3Al−1.5Y | 204±5.3 | 16.8±5.0 | 248±7.2 | 27.1±4.6 |
| Mg−4Li−3Al−2Y | 159±4.8 | 11.2±3.2 | 226±3.0 | 22.6±4.8 |

significantly. According to Table 5, Mg−4Li−3Al−0.5Y alloy maintains the highest UTS, while the largest elongation is obtained in Mg−4Li−3Al−1.5Y alloy. Although 1.0−1.5 wt.% Y addition does not produce large improvement of UTS of hot extruded Mg−4Li−3Al alloy, the Y addition indeed contributes to a higher elongation and the largest elongation is obtained in hot-extruded Mg−4Li−3Al−1.5Y alloy.

## 4 Discussion

### 4.1 Effect of Y on microstructures

Y is an effective grain refiner for Mg−Li−Al alloys. The solubility of Y in Mg (3.4 at.% at 567.4 °C) is large. Addition of Y in Mg−Li−Al alloys results in the formation of $Al_2Y$ compound due to the highest electronegativity difference between Al (1.66) and Y (1.20). $Al_2Y$ compound precipitates with high melting point (1758 K) are preferentially formed and provide nucleating sites for solidification of $\alpha$-Mg. $Al_2Y$ compound hinders grain growth by pinning grain boundaries, which leads to decreasing grain size in Mg−Li−Al ingots with Y addition. In the present study, the average grain size of $\alpha$-Mg matrix in Mg−4Li−3Al ingots is significantly decreased when 1 wt.% Y is added. However, the value of average grain size remains stable when the Y content is ≥1.0 wt.%. Microstructure evolution suggests that $Al_2Y$ phase is aggregated and transforms from particles to block-like shape with the continuous addition of Y, which weakens the grain refining effect and is responsible for the stable average grain size in Mg−Li−Al ingots with 1−2 wt.% Y addition.

In addition, dynamic recrystallization (DRX) of Mg−Li−Al alloys is also affected by Y addition and fine equiaxed grains in Mg−Li−Al alloys with Y addition are the result of DRX during hot extrusion. The effect of Y element on DRXed microstructure of magnesium alloys is generalized into two ways. Firstly, fine and dispersive $Al_2Y$ particles provide nucleus of new DRX grains during nucleation and promote DRX process of magnesium [20]. Secondly, $Al_2Y$ particles can restrain the growth of DRX grains by hindering the migration of grain boundaries. TANG et al [19] showed that the $Al_2Y$ particles could promote DRX process in Mg alloys during hot deformation, attributed to the decrease of stacking fault energy after adding rare earth elements and PSN (particle stimulated nucleation) process due to $Al_2Y$. In Mg−4Li−3Al−2Y alloy with 2.0 wt.% Y content, the amount and average size of $Al_2Y$ particles increase simultaneously. The aggregative large $Al_2Y$ particles cannot provide more nucleus nor effectively impede grain growth during DRX. Hence, coarse grains are obtained in Mg−4Li−3Al−2Y alloy. Therefore, the smallest average grain size is obtained in hot-extruded Mg−4Li−3Al−1.5Y alloy.

Besides grain refinement, previous studies indicated that RE addition weakened basal textures in magnesium alloys by modification of stacking fault energy (SFE) of $\alpha$-Mg matrix and solute drag/pinning effect. SANDLÖBES et al [23] measured the partial dislocation of cold-rolled Mg−3wt.%Y alloy by transmission electron microscopy (TEM) and calculated the energy of the intrinsic basal $I_1$ stacking fault. They found a significant decrease in the intrinsic stacking fault $I_1$ energy ($I_1$ SFE) with the addition of Y. They also conducted calculations by using density functional theory, which showed that the $I_1$ SFE of Mg was decreased almost linearly with the addition of Y. Low SFE promotes dislocation dissociation reactions, which reduces the probability of climb and cross-slip for basal dislocation, retarding the

dynamic recovery of metallic materials [24,25]. Since the atomic radius of RE elements is much larger than that of Mg (more than 10%), RE elements in magnesium alloys have a strong tendency at segregate to grain boundaries (GBs) or defect sites to reduce the size misfit energy in the Mg matrix [16]. ROBSON [26] demonstrated that a wide range of RE elements was predicted to segregate strongly at grain boundaries due to the large atomic size misfit with magnesium. According to his results, segregated Y was predicted to produce a solute drag pressure on migrating boundaries by several orders of magnitude greater than that obtained by Al or Zn additions, due to both the high tendency of Y to segregate at boundaries and the low diffusivity of Y in Mg. JUNG et al [16] suggested that this Y segregation was responsible for the strong suppression of dynamic recrystallization (DRX) in Mg−Y alloys. In the present study, the average grain size of Mg−Li−Al alloys decreases with increasing Y content until the Y content is 1.5 wt.%. Fine and homogenous grain structure is obtained in Mg−4Li−3Al−1.5Y alloy due to decreased SFE and solute drag/pinning effect of Y during DRX. As seen in Figs. 4(e) and 5(e), the size and amount of $Al_2Y$ particles in Mg−4Li−3Al alloys with 2 wt.% Y both increase. Large and segregated $Al_2Y$ particles cannot provide more nucleation sites for DRX grains during hot extrusion, which retards the DRX progress of Mg−4Li−3Al−2Y alloy. On the other hand, the solid solubility of alloying elements in the matrix might be reduced due to the formation of $Al_2Y$ phase, which will weaken the solute dragging effect. Therefore, grains become coarser when the Y content is increased to 2 wt.%, which is ascribed to inefficient retarding DRX effect related to the formation of large and aggregative $Al_2Y$ particles in Mg−4Li−3Al−2Y alloy.

### 4.2 Effect of Y on mechanical properties

The addition of Y into magnesium alloys has been reported to be a good strategy to achieve high ductility and strength at both room and high temperature as well as creep resistance [27]. The improvement of mechanical properties of Mg−4Li−3Al alloy can be ascribed to solution strengthening, dispersion strengthening and grain refinement effects. First of all, as discussed above, the solubility of Y in Mg is large, and large amounts of Y atoms exist in Mg−4Li−3Al alloy by the formation of solid solution. Therefore, the improvement of strength of Mg−4Li−3Al alloy is obtained by solid solution strengthening. Secondly, Y addition into Mg−Li−Al alloys introduces $Al_2Y$ phases with a high thermal stability and hardness and $Al_2Y$ phases are broken into small particles dispersing in the $\alpha$-Mg matrix, which leads to the strength improvement by precipitation strengthening. Finally, $Al_2Y$ is confirmed to be an effective grain refiner and it also contributes to promoting DRX of magnesium alloys during hot extrusion [27]. Fine and equiaxed grains are obtained in Mg−4Li−3Al alloys with Y addition, especially in Mg−4Li−3Al−1.5Y alloy. It is well known that grain refinement is an excellent strategy to improve strength and ductility simultaneously. Based on discussion above, it is reasonable to expect both high strength and large elongation in Mg−4Li−3Al−1.5Y alloy. It should be also noted that the elongation of Mg−4Li−3Al−1.5Y alloy is the highest among all the as-extruded Mg−4Li−3Al alloys. As discussed above, the ductility of metallic materials can be achieved by grain refinement. Table 3 and Fig. 6 indicate that the average grain size of Mg−4Li−3Al−1.5Y alloy has the smallest value. Therefore, higher ductility should be expected in this alloy. Furthermore, the solid solubility of Y is considered to be increased with increasing Y content in Mg−4Li−3Al alloys. Increased ductility from a significantly larger amount of slip with $\langle c+a \rangle$ components in Y-alloyed Mg was reported in Ref. [28]. According to their results, due to the enhanced activity of non-basal deformation modes, Mg−Y alloy can accommodate a larger amount of strain applied by homogeneous deformation [28]. Synergy of grain refinement and enhanced activity of non-basal slips bring about the highest elongation of Mg−4Li−3Al−1.5Y alloy. Compared with Mg−4Li−3Al alloy with 1.5 wt.% Y, the UTS of Mg−4Li−3Al−2Y alloy is decreased significantly. Coarser grains and larger $Al_2Y$ particles are considered to deteriorate the strength of Mg−4Li−3Al−2Y alloy. According to Fig. 6 and Table 3, the average grain size of as-extruded Mg−4Li−3Al−2Y alloy is the largest. Besides, Figs. 4(e) and 5(e) demonstrate that there are lots of large $Al_2Y$ particles, which will induce stress localization around these particles. During tensile deformation, cracks initiate and propagate along

large particles, and lead to final failure of Mg−4Li−3Al−2Y alloy.

Detailed investigation of Fig. 8 indicates that serrated flow occurs at large strain (>~10%) on the engineering strain−stress curves of Mg−4Li−3Al alloys. Two prevailing mechanisms concerning serrated flow has been reported: one is the theory of dynamic strain aging, which attributed serrated flow to the dynamic interaction between solute atoms and dislocations; the other is the shearing of precipitates by dislocations [29]. WANG et al [29] observed serrated flow of a Mg−Li alloy (LA41 magnesium alloy) and explained this phenomena through the competition between the shearing of precipitates by dislocations and dynamic strain aging. $Al_2Y$, AlLi and $MgLiAl_2$ are formed in Mg−4Li−3Al alloys, and these large particles hinder the movement of dislocations. With deformation proceeding, piled dislocations may shear fine particles, and stress concentration is relaxed temporarily. During plastic deformation, piling up of dislocations and shearing of precipitates alternate, and macroscopic serrations are detected on the engineering strain−stress curves of Mg−4Li−3Al alloys.

## 5 Conclusions

(1) Mg−4Li−3Al alloys consist of single $\alpha$-Mg matrix and $Mg_{17}Al_{12}$, AlLi, $MgLi_2Al$ phases. After Y addition, $Al_2Y$ particles are revealed in $\alpha$-Mg matrix in as-cast Mg−4Li−3Al alloys.

(2) Grains of as-cast Mg−4Li−3Al alloys with Y addition are dramatically refined and the mechanical properties of alloys with Y addition are significantly improved due to hot extrusion process. The average grain size of hot-extruded Mg−4Li−3Al−1.5Y is the smallest (~8.5 μm).

(3) Hot extruded Mg−4Li−3Al−1.5Y alloy possesses a good combination of ultimate tensile strength (UTS=248 MPa) and elongation ($\delta$=27%). The improvement of mechanical properties in hot-extruded Mg−4Li−3Al alloys with Y addition is mainly attributed to grain refinement, solid solution strengthening, and precipitates strengthening.

## Acknowledgments

The work was supported by the National Natural Science Foundation of China (No. 51401115), the Promoted Research Fund for Excellent Young and Middle-aged Scientists of Shandong Province, China (No. BS2013CL034) and partially by the Fundamental Research Funds of Shandong University, China (2016JC016).

## Data availability

The raw/processed data required to reproduce these findings cannot be shared at this time as the data also form part of an ongoing study.

## References

[1] KIM Y H, KIM J H, YU H S, CHOI J W, SON H T. Microstructure and mechanical properties of Mg−*x*Li−3Al−1Sn−0.4Mn alloys (*x*=5, 8 and 11 wt.%) [J]. Journal of Alloys and Compounds, 2014, 583: 15−20.

[2] DONG Han-wen, WANG Li-dong, WU Yao-ming, WANG Li-min. Effect of Y on microstructure and mechanical properties of duplex Mg−7Li alloys [J]. Journal of Alloys and Compounds, 2010, 506: 468−474.

[3] CUI Chong-liang, WU Li-bin, WU Rui-zhi, ZHANG Jing-huai, ZHANG Mi-lin. Influence of yttrium on microstructure and mechanical properties of as-cast Mg−5Li−3Al−2Zn alloy [J]. Journal of Alloys and Compounds, 2011, 509: 9045−9049.

[4] ZHANG Cheng, WU Liang, ZHAO Zi-long, XIE Zhi-hui, HUANG Guang-sheng, LIU Lei, JIANG Bin, ATRENS A, PAN Fu-sheng. Effect of Li content on microstructure and mechanical property of Mg−*x*Li−3(Al−Si) alloys [J]. Transactions of Nonferrous Metals Society of China, 2019, 29: 2506−2513.

[5] SUN Yue-hua, WANG Ri-chu, PENG Chao-qun FENG Yan, YANG Ming. Recent progress in Mg−Li matrix composites [J]. Transactions of Nonferrous Metals Society of China, 2019, 29: 1−14.

[6] CHEN Xiao-yang, ZHANG Yang, CONG Meng-qi, LU Ya-lin, LI Xiao-ping. Effect of Sn content on microstructure and tensile properties of as-cast and as-extruded Mg−8Li−3Al−(1,2,3)Sn alloys [J]. Transactions of Nonferrous Metals Society of China, 2020, 30: 2079−2089.

[7] ZHAO Jiong, ZHANG Jie, LIU Wen-cai, WU Guo-hua, ZHANG Liang. Effect of Y content on microstructure and mechanical properties of as-cast Mg−8Li−3Al−2Zn alloy with duplex structure [J]. Materials Science and Engineering A, 2016, 650: 240−247.

[8] HE Yu-ding, PENG Chao-qun, FENG Yan, WANG Ri-chu, ZHONG Jian-feng. Effects of alloying elements on the microstructure and corrosion behavior of Mg−Li−Al−Y alloys [J]. Journal of Alloys and Compounds, 2020, 834: 154344−154344.

[9] ZHAO Zi-long, SUN Zi-wei, LIANG Wei, WANG Yi-de, BIAN Li-ping. Influence of Al and Si additions on the microstructure and mechanical properties of Mg−4Li alloys [J]. Materials Science and Engineering A, 2017, 702: 206−217.

[10] CHANG T C, WANG J Y, CHU C L, LEE S. Mechanical properties and microstructures of various Mg−Li alloys [J].

Materials Letters, 2006, 60: 3272−3276.
[11] SANSCHAGRIN A, TREMBLAY R, ANGERS R, DUB D. Mechanical properties and microstructure of new magnesium-lithium base alloys [J]. Materials Science and Engineering A, 1996, 220: 69−77.
[12] XIANG Q, WU R Z, ZHANG M L. Influence of Sn on microstructure and mechanical properties of Mg−5Li−3Al−2Zn alloys [J]. Journal of Alloys and Compounds, 2009, 477: 832−835.
[13] DROZD Z, TROJANOV Z, KUDELA S. Deformation behaviour of Mg−Li−Al alloys [J]. Journal of Alloys and Compounds, 2004, 378: 192−195.
[14] TANG Yan, JIA Wei-tao, LIU Xuan, LE Qi-chi, CUI Jian-zhong. Precipitation evolution during annealing of Mg−Li alloys [J]. Materials Science and Engineering A, 2017, 689: 332−344.
[15] ISLAM R, HADADZADEH A, WELLS M, HAGHSHENAS M. Characterization and analysis of hot compression behaviors of an ultralight Mg−Li−Al alloy [J]. International Journal of Lightweight Materials and Manufacture, 2019, 2: 217−226.
[16] JUNG I H, SANJARI M, KIM J, YUE S. Role of RE in the deformation and recrystallization of Mg alloy and a new alloy design concept for Mg−RE alloys [J]. Scripta Materialia, 2015, 102: 1−6.
[17] MINAEI K P, DROZDENKO D, ZEMKOV A M, VESEL Y J, ČAPEK J, BOHLEN J, DOBROŇ P. Advanced analysis of the deformation mechanisms in extruded magnesium alloys containing neodymium or yttrium [J]. Materials Science and Engineering A, 2019, 759: 455−464.
[18] MISHRA R K, GUPTA A K, RAO P R, SACHDEV A K, KUMAR A M, LUO A A. Influence of cerium on the texture and ductility of magnesium extrusions [J]. Scripta Materialia, 2008, 59: 562−565.
[19] TANG Wei-qin, ZHOU Guo-wei, SHAO Yi-chuan, LI Da-yong, PENG Ying-hong, WANG Hua-miao. On the role of yttrium in microstructure evolution and texture modification during magnesium alloy extrusion [J]. Materials Characterization, 2020, 162: 110189−110189.
[20] HANTZSCHE K, BOHLEN J, WENDT J, KAINER K U, YI S B, LETZIG D. Effect of rare earth additions on microstructure and texture development of magnesium alloy sheets [J]. Scripta Materialia, 2010, 63: 725−730.
[21] HUANG Y S, TSAO C S, WU S K. Evolution and growth kinetics of θ precipitates in naturally aged MgLiAlZn alloy studied by in situ small-angle X-ray scattering [J]. Metallurgical and Materials Transactions A: Physical Metallurgy and Materials Science, 2019, 50: 1949−1956.
[22] LIU T, WU S D, LI S X, LI P J. Microstructure evolution of Mg−14%Li−1%Al alloy during the process of equal channel angular pressing [J]. Materials Science and Engineering A, 2007, 460−461: 499−503.
[23] SANDOBES S, FRIAK M, ZAEFFERER S, DICK A, YI S, LETZIG D, PEI Z, ZHU L F, NEUGEBAUER J, RAABE D. The relation between ductility and stacking fault energies in Mg and Mg−Y alloys [J]. Acta Materialia, 2012, 60: 3011−3021.
[24] HUANG K, LOG R E. A review of dynamic recrystallization phenomena in metallic materials [J]. Materials & Design, 2016, 111: 548−574.
[25] LONG L J, HUANG G H, YIN D D, JI B, ZHOU H, WANG Q D. Effects of Y on the deformation mechanisms of extruded Mg−Y sheets during room-temperature compression [J]. Metallurgical and Materials Transactions A: Physical Metallurgy and Materials Science, 2020, 51: 2738−2751.
[26] ROBSON J D. Effect of rare-earth additions on the texture of wrought magnesium alloys: The role of grain boundary segregation [J]. Metallurgical and Materials Transactions A, 2014, 45: 3205−3212.
[27] QIU D, ZHANG M, TAYLOR J, KELLY P. A new approach to designing a grain refiner for Mg casting alloys and its use in Mg−Y-based alloys [J]. Acta Materialia, 2009, 57: 3052−3059.
[28] SANDLOBES S, ZAEFFERER S, SCHESTAKOW I, YI S, GONZALEZ-MARTINEZ R. On the role of non-basal deformation mechanisms for the ductility of Mg and Mg−Y alloys [J]. Acta Materialia, 2011, 59: 429−439.
[29] WANG Cong, XU Yong-bo, HAN En-hou. Serrated flow and abnormal strain rate sensitivity of a magnesium−lithium alloy [J]. Materials Letters, 2006, 60: 2941−2944.

# Y 对 Mg−4Li−3Al 合金显微组织演变及力学性能的影响

常丽丽，郭 晶，苏效婧

山东大学 材料科学与工程学院，济南 250061

**摘 要**：为制备轻质高性能镁合金，将稀土元素 Y 添加至 Mg−4Li−3Al (质量分数，%)合金。采用金相显微镜、扫描电子显微镜及拉伸试验研究 Y 含量对于 Mg−4Li−3Al 合金显微组织演变与力学性能的影响。研究发现，铸态 Mg−4Li−3Al 合金的力学性能经挤压后得到显著提高。热挤压 Mg−4Li−3Al−1.5Y 合金的综合力学性能最优，抗拉强度为 248 MPa、伸长率为 27%。热挤压 Mg−4Li−3Al−1.5Y 合金的力学性能提升是晶粒细化、固溶强化和析出相强化协同作用的结果。

**关键词**：Mg−Li−Al 合金；Y 元素；显微组织；极限抗拉强度；伸长率

**(Edited by Bing YANG)**